Identification and visualization of oxidized lipids in atherosclerotic plaques by microscopic imaging mass spectrometry-based metabolomics

Lianhua Shen[1,3,4], Takushi Yamamoto[6], Xian Wen Tan[2], Koretsugu Ogata[6], Eiji Ando[6], Eiichi Ozeki[4], Eiji Matsuura[1, 2, 5*]

[1] Collaborative Research Center (OMIC) and [2] Department of Cell Chemistry, Okayama University Graduate School of Medicine, Dentistry, and Pharmaceutical Sciences, 2-5-1 Shikata-cho, Kita-ku, Okayama 700-8558, Japan

[3] Department of Pathophysiology, Zunyi Medical University, 6 West Xuefu Road, Xinpu District, Zunyi City, Guizhou, 563003, China

[4] Technology Research Laboratory, Shimadzu Corporation, 3-9-4 Hikaridai, Seika-cho, Soraku-gun, Kyoto 619-0237, Japan

[5] Neutron Therapy Research Center, Okayama University, 2-5-1 Shikata-cho, Kita-ku, Okayama 700-8558, Japan

[6] Analytical & Measuring Instruments Division, Shimadzu Corporation, 1 Nishinokyo, Kuwabara-cho, Nakagyo-ku, Kyoto 604-8511, Japan

*****Corresponding author:

Eiji Matsuura

Email: eijimatu@md.okayama-u.ac.jp

Abstract

Background and aims: Dysregulated lipid metabolism has emerged as one of the major risk factors of atherosclerosis. Presently, there is a consensus that oxidized LDL (oxLDL) promotes development of atherosclerosis and downstream chronic inflammatory responses. Due to the dynamic metabolic disposition of lipoprotein, conventional approach to purify bioactive lipids for subsequent comprehensive analysis has proven to be inadequate for elucidation of the oxidized lipids species accountable for pathophysiology of atherosclerotic lesions. Herein, we aimed to utilize a novel mass microscopic imaging technology, coupled with mass spectrometry (MS) to characterize oxidized lipids in atherosclerotic lesions.

Methods: We attempted to use MALDI-TOF-MS and iMScope to identify selected oxidized lipid targets and visualize their respective localizations in study models of atherosclerosis.

Results: Based on the MS analysis, detection of 7-K under positive ionization through product ion peak at *m/z* 383 [M+H-H_2O] indicated the distinctive presence of targeted lipid within Cu^{2+}-oxLDL and Cu^{2+}-oxLDL loaded macrophage-like J774A.1 cell, along with other cholesterol oxidation products. Moreover, the application of two-dimensional iMScope has successfully visualized the localization of lipids in aortic atherosclerotic plaques of the Watanabe heritable hyperlipidemic (WHHL) rabbit. Distinctive lipid distribution profiles were observed in atherosclerotic lesions of different sizes, especially the localizations of lysoPCs in atherosclerotic plaques.

Conclusions: Taken together, we believe that both MALDI-TOF-MS and iMScope metabolomics technology may offer a novel proposition for future pathophysiological studies of lipid metabolism in atherosclerosis.

Keywords: Atherosclerosis, Low-density lipoprotein (LDL), Oxidized LDL (oxLDL), Oxidized lipids, Imaging mass microscopy (iMScope), Mass spectroscopy (MS)

Introduction

Metabolic abnormalities of lipoproteins have an intimate involvement in the pathogenicity of lifestyle diseases, such as cardiovascular diseases and diabetes mellitus [1]. Low-density lipoprotein (LDL), that contains cholesterol and cholesteryl esters (CEs) at nearly 50 % of its composition, is most susceptible to oxidative damage than other lipoproteins. The oxidation of native LDL (nLDL) into oxidized LDL (oxLDL) is generated by reactive oxygen species (ROS), such as superoxide anions or hydroxyl radicals in the blood vessels [2].

The lipid components of an oxLDL particle generally include CEs, sterols, oxysterols (oxygenated derivatives of cholesterol), phospholipids, lysophosphatidylcholine (lyso-PC), 9-hydroxyoctadecadienoate (9-HODE), 13-hydroxyoctadecadienoate (13-HODE), hydroxyl fatty acids, *etc.* [3, 4]. Among all, oxysterols are allegedly the most toxic components of oxLDL [5, 6]. They exist in human atherosclerotic plaques and actively involved in plaque development [7, 8]. 7-ketocholesterol (7-K), coming in second after 27-hydroxycholesterol (27-OH), is one of the most abundant forms of oxysterol detected in human atherosclerotic plaques. It is formed non-enzymatically from the intermediate by-product of cholesterol oxidation, 7-hydroperoxycholesterol (7-OOH), and it carries a ketone functional group. The involvement of 7-K in manifestation of atherosclerosis has been apparent. It emerged as a potent apoptotic inducer to which the embodiment of 7-K to lipid raft domains of plasma membranes has been reported to propagate apoptotic signals [9, 10].

In plasma, the majority of the cholesterols and their oxidized forms, oxysterols, exist in esterified forms. Approximately 75% of the linoleic acid in LDL exists in esterified form, as a CE of linoleic acid (CE 18:2) [11, 12]. The CE 18:2 is subsequently converted to hydroxy-octadecadienoate-CE (HODE-CE) following the reduction of its initial hydroperoxide product, the hydroperoxy-octadecadieoate-CE (HpODE-CE) [12, 13], the oxo-octadecadienoate-CE (oxoODE-CE), as well as the chain-shortened ω-aldehyde-CE, often referred as “core

aldehydes" [14-16]. These severely oxidized CE (oxCE) were detected and have been shown to accumulate in human atheroma and human plasma [15, 17, 18]. In Cu^{2+}-oxidized LDL, 9-oxononanoylcholesterol (9-ONC) exists as a major form of oxCE [19] and subsequent oxidation of its cholesterol backbone resulted in formation of 7-ketocholesteryl-9-carboxynonanoate (oxLig-1). Our previous studies have reported that the oxCE-based oxidant associated with the onset of autoimmunity and atherosclerosis was identified as oxLig-1 and its downstream signaling pathways involving CD36 were reported [20-22].

β2-glycoprotein I (β2GPI) is a glycoprotein that is known to bind specifically to hydrophobic anionic moieties such as oxLDL and has been shown to dose-dependently inhibit the scavenger receptor-mediated uptake of oxLDL by macrophages [23]. In addition, immunization of *Ldlr* knockout (*Ldlr*$^{-/-}$) mice with β2GPI was reported to promote formation of atherosclerotic plaque with extensive localization of glycoprotein at the plaque legions [24]. Our previous studies reported that β2GPI binds electrostatically to oxLDL and form oxLDL/β2GPI complexes through specific ligands, known as oxLig-1. OxLig-1 is structurally consisting of 7-K and an acyl chain with a terminal carboxyl group (Supplementary Fig. 1).

Our previous studies have substantiated the functions of these oxLDL/β2GPI complexes as major atherogenic and thrombogenic autoantigens in patients with the antiphospholipid syndrome. These complexes were also detected in patients with diabetes mellitus and chronic renal diseases [23, 25-28]. In addition, we have demonstrated that the uptake of oxLDL/β2GPI complexes by macrophages (through its Fcγ receptors) was significantly enhanced in the presence of anti-oxLDL/β2GPI IgG autoantibodies and has notably accelerated the formation of foam cells and progression of atherosclerosis [27, 29-32].

Inflammation plays a key role in physiological oxidation and degeneration of lipoproteins. The constant shifting of lipoprotein particle size and its dynamic metabolic disposition have limited the application of conventional approach to purify bioactive lipids for subsequent

comprehensive analysis. As such, the novel method of utilizing imaging mass microscope (iMScope) system with MS/MS imaging for direct detection and identification of bioactive lipids is deem pivotal to elucidate the pathology of atherosclerosis. iMScope is a novel imaging mass spectrometry, composed of an optical microscope and a hybrid ion trap time of flight mass spectrometer. The system has a resolution of 5 μm and capable of visualizing the distribution of molecules at sub-cellular level. Herein, our present work focused on the establishment of novel iMScope and MS/MS imaging metabolomic technology to characterize different oxidized lipids in atherosclerotic lesions. The distributions of oxidized lipids in the aortic lesions were thoroughly visualized with iMScope and elucidated by MS/MS imaging technology. Such novel approach may offer new method to comprehensively unravel the pathophysiology of atherosclerosis in the context of lipids.

Materials and methods

Chemicals and reagents

Mass spectrometry grade chemicals and reagents were used in the present study. 2, 5-dihydroxybenzoic acid (DHB) was purchased from Shimadzu GLC Ltd (Kyoto, Japan). Lipid moieties inclusive of 27-hydroxycholesterol (27-OH), 25-hydroxycholesterol (25-OH), 7-ketocholesterol (7K), N-palmitoyl-D-erythro-sphingosylphosphorylcholine [SM34:1, (d18:1/16:0)], phosphatidylcholine 16:0/16:0 (DPPC) and phosphatidylcholine (PC) 16:0/18:2 were purchased from Avanti Polar Lipids Inc. (Alabaster, AL). Cholesterol, 7β-Hydroxycholesterol (7β-OH) and cholesteryl linoleate (CE 18:2) were obtained from Sigma-Aldrich Japan G.K. (Tokyo, Japan). 9(R)-HODE cholesteryl ester or (±) 13-HODE cholesteryl ester (HODE-CE), and cholesteryl linoleate hydroperoxides (oxo-octadecadienoate-CE, oxoODE-CE) were purchased from Cayman Chemical Company (Ann Arbor, MI). OxLig-1 was synthesized in-house as described previously [20] and the structure was verified by MALDI-TOF-MS/MS analysis.

Animal Studies

The study was adhered to the Ethical Committee's Guidelines for Animal Research at Okayama University. Twelve atherosclerosis-prone mouse strains, *Ldlr*$^{-/-}$ mice, with a $C_{57}BL/_{6}$ genetic background (Jackson Laboratories, Bar Harbor, ME) were used and their genotypes were verified via polymerase chain reaction (PCR). After 8 weeks of age, mice were fed with high-fat diet (containing cholic acid) for 8 weeks. Mice were then sacrificed to harvest the whole blood for isolation of LDL. One Watanabe heritable hyperlipidemic (WHHL) rabbit (Brown Family Enterprises, LLC., Odenville, AL) was fed with the regular rabbit diet for 6 months and sacrificed to harvest the thoracic aorta. The collected specimen was embedded in O.C.T. compound, froze in liquid nitrogen, and stored at -80 °C.

Isolation and oxidation of LDL

The LDL fraction was collected from fresh plasma of high-fat diet-fed *Ldlr*$^{-/-}$ mice (16 weeks old, n=12) by ultracentrifugation, as described previously [33]. LDL was then oxidized with 5 μM of $CuSO_4$ for 16 hours at 37 °C. Oxidation was terminated by addition of EDTA to the reaction mixture (at a final concentration of 1 mM). The oxidized LDL fraction was dialyzed against 1 mM EDTA in PBS buffer overnight at 4 °C. The degree of oxidation was estimated via the thiobarbituric acid reactive substances (TBARS) assay and expressed in nmol malondialdehyde (MDA) equivalent per mg protein.

MALDI-TOF-MS

The MALDI-TOF-MS (AXIMA-Performance; Shimadzu Corporation) equipped with nitrogen pulsed UV laser (337 nm) was operated using a positive ion source in 'Reflectron' mode and the laser power was set at 90 mV. Each spot was analyzed using a random raster of 200 profiles, and each profile consisted of data from five laser shots. The data were collected with the Launchpad 2.8 software (Shimadzu Corporation). The *m/z* values were externally calibrated using DHB matrix with human bradykinin fragment 1-7 and angiotensin II as peptide calibration standards (Sigma-Aldrich Japan G.K., Tokyo, Japan). The identification of lipids prepared from Cu^{2+}-oxLDL was confirmed by MALDI-TOF-MS/MS with reference to product ion spectra of authentic lipid standards.

Cell culture and intracellular lipid accumulation assay

Intracellular lipid accumulation was studied by using murine macrophage-like cell line, J774A.1 (Riken Cell Bank, Tsukuba, Japan). The cells were maintained in RPMI-1640 medium supplemented with 10% FBS. The cells were seeded onto 24-well culture plates at a density of $1x10^5$ cells/ml/well and were incubated at 37 °C, along with 20 μg/ml *Ldlr*$^{-/-}$ mice-derived

nLDL or copper sulfate-modified oxLDL (Cu^{2+}-oxLDL) for 6 hours. After incubation, the cells were washed with PBS, collected by centrifugation, and spotted onto the indium tin oxide (ITO)-coated conductive glass slide (Sigma-Aldrich Japan G.K., Tokyo, Japan). The sample was then mounted with DHB solution, dried and directly analyzed by MALDI-TOF-MS.

Tissue section preparation

Frozen WHHL rabbit aorta was sectioned at 10 μm thickness using Cryostat Leica CM1860 (Leica Microsystems, Solms, Germany). Several serial sections were mounted onto: (i) The MAS-coated glass slides (Matsunami Glass Industries, Osaka, Japan) for histochemical staining, and (ii) ITO-coated conductive glass slide for iMScope. Specimens were stored in slide chamber at kept at -80 °C until use.

Histochemical staining

The frozen serial tissue sections were stained with Oil Red O for visualization of neutral lipids. The counterstaining of nucleus was performed with the Mayer's hematoxylin solution (Wako Pure Chemical Industries, Ltd., Osaka, Japan). Bright field microscopy images of Oil Red O stained tissue sections were obtained by Keyence BZ-X700 All-in-one Fluorescence Microscope (Keyence Corporation, Itasca, IL).

Visualization of lipids distributions in aortic lesions by imaging mass microscope (iMScope)

A total of 50 mg/mL of DHB [reconstituted in methanol/1% TFA/distilled water (7:1:2, v/v)] was used as a matrix. The prepared sample glass slides were spray-coated with 500 μL DHB matrix solutions via a 0.3 mm nozzle caliber airbrush (Procon Boy FWA Platinum; GSI Creos Co., Tokyo, Japan). Thereafter, the glass slides were vacuum-dried, and followed by visualization of lipid distributions with iMScope. iMScope was performed using 1,000 Hz solid laser. A 10 μm pitch of special resolution was used, and the data were acquired in positive

ionization. The *m/z* values in the mass range of 350-800 were measured and were internally calibrated with DHB. All the spectra were acquired using atmospheric pressure MALDI (Shimadzu Corporation). The spectra were normalized based on total ion current (TIC) to eliminate variations in ionization efficiency, by using the Imaging MS Solution 1.01.00 software (Shimadzu Corporation). Substances in specified regions were compared by Region of Interest (ROI) analysis and the differences in areas within ROI were analyzed by the Welch's *t*-test. The identities of lipids were further confirmed by MALDI-MS/MS with reference to authentic lipid standards.

Statistical analysis

Statistical significance with p-value of less than 0.05 was considered as statistically significant. The p-value of comparison for region of interest (ROI) analyses was assessed via average peak intensities or signals acquired from MS spectra of areas indicated by ROI. Low p-values ($p < 0.05$) denotes significant differences between average peak intensities or signals of targets within the stipulated ROIs.

Results

Analysis of oxidized lipids from lipoprotein fractions by MALDI-TOF-MS

Oxidation rate of LDL was evaluated via TBARS assay. A distinct difference in MDA content between nLDL and oxLDL was observed. nLDL recorded 4 nmol MDA equivalent/mg protein while oxLDL recorded 220 nmol MDA equivalent/mg protein (Supplementary Fig. 2). These observations highlighted the oxidation of nLDL into oxLDL. MS profiles of cholesterol and related oxidized lipid reference standards were first set-up by using authentic standards (Supplementary Fig. 3). The reference mass profile of different oxidized lipids is shown in Supplementary Fig. 3. 7-K was detected as protonated precursor ions at *m/z* 401 $[M+H]^+$ and

m/z 423 $[M+Na]^+$, respectively. As for oxLig-1, it was detected at *m/z* 593 as a sodium adduct ion $[M+Na]^+$.

The MS profiles of derived nLDL and Cu^{2+}-oxLDL are shown in Supplementary Fig. 4. Potential identity of oxidized lipids detected in mice-derived lipoprotein fractions was then determined with reference to MS profiles of authentic standards. The results showed that the oxidation products of cholesterol and its ester were detected only in Cu^{2+}-oxLDL. Product ion peak at *m/z* 383 $[M+H-H_2O]^+$ was derived from 7-K and oxLig-1; these MS fingerprints were comparable to the MS profiles of authentic standards. In addition, the presence of "molecule A" in *Ldlr*$^{-/-}$ mice derived Cu^{2+}-oxLDL were postulated as oxysterols such as 27-OH, 25-OH or 7-OH, which were detected at *m/z* 385 $[M+H-H_2O]^+$ and *m/z* 367 $[M+H-2H_2O]^+$, respectively (Supplementary Fig. 4A).

Contrarily, cholesterol and cholesterol linoleate (CE 18:2) were detected in both nLDL and Cu^{2+}-oxLDL (Supplementary Fig. 4A and B). The product ion of cholesterol was detected at *m/z* 369 $[M+H-OH]^+$ while CE 18:2 was detected as protonated precursor ion at *m/z* 671 $[M+Na]^+$. By comparing the MS spectra of two different lipoprotein fractions, CE 18:2 existed abundantly in nLDL fraction while its abundance was notably reduced in the oxidized lipoprotein fraction. Meanwhile two oxCEs of CE 18:2: 9-HODE-CE and oxoODE-CE, were detected only in Cu^{2+}-oxLDL with the identified protonated precursor ions peaks at *m/z* 687 and *m/z* 685 respectively, as $[M+Na]^+$ adduct ion (Supplementary Fig. 4B).

In addition, we have also identified several biological membranous lipids including SM34:1, phosphatidylcholine (PC) 32:0 (16:0/16:0) and PC 34:2 (16:0:18:2). The presence of these biological membranous lipids were confirmed in both nLDL and oxLDL lipid fractions at *m/z* 703, *m/z* 734 and *m/z* 758, respectively (Supplementary Fig. 4C).

From these results, we concluded that the MS profiles of specific molecular ions acquired from oxidized lipids, such as 7-K ion, was specifically detected only in Cu^{2+}-oxLDL derived

from sera of the knock-out mice. Contrarily, direct detection of full length oxLig-1 from Cu^{2+}-oxLDL by MALDI-TOF-MS was constrained. Characteristic MS fingerprint of oxLig-1 (at *m/z* 593) was not detected in both lipid fractions. Hence, an alternative study model involving the use of murine macrophage-like J774A.1cells was employed to detect the presence of oxLig-1 in Cu^{2+}-oxLDL.

Phagocytosis of oxLDL by murine macrophage-like cell line, J774A.1

Brown AJ et. al. (2000) indicated that both cholesterol and 7-K, along with their esters were assessable in macrophages loaded with modified lipoproteins [34]. In this study, the J774A.1 cells were used as an *in vitro* study model to evaluate the intracellular lipid accumulation of oxidized lipids. Detection of oxidized lipids from the cells was then performed by MALDI-TOF-MS (Fig. 1A). The MS spectra of nLDL and Cu^{2+}-oxLDL were obtained from the macrophage pre-incubated with either nLDL or Cu^{2+}-oxLDL at final concentrations of 20 μg/ml for 6 hours. The detected MS profiles of oxidized lipids derived from Cu^{2+}-oxLDL treated J774A.1 cells (Fig. 1B) were comparable to that derived from Cu^{2+}-oxLDL fraction (Supplementary Fig. 4). Yet, the obtained spectral signal of oxLig-1 was weak and thus limiting its identification by MS/MS.

MS imaging of cholesterol oxidation process on atherosclerosis plaque in WHHL Rabbit

The distributions of lipids and their associated oxidized forms in atherosclerotic plaque were visualized by the novel iMScope with a MS imaging technology. Direct detections of lipids obtained from atherosclerosis plaque were made possible without the utilization of antibody or extensive purification steps. Fig. 2 shows the optical microscopic image and MS visual mappings of lipids and oxidized lipids on two regions of sectioned aortic tissues from WHHL rabbits.

The two regions of interest of sectioned aortic tissue (shown in Fig. 2) consisted of atherosclerotic lesions of different sizes: large (Fig. 2A) and small lesions (Fig. 2B). Both Fig. 2A and B depicted the visual mappings of different lipid targets. The targeted lipids include: (a) cholesterol; (b) CE 18:2; (c) PCs (PC 32:0, PC 34:2, PC 37:4, PC 36:2); (d) SMs [SM 34:1 (18:1/16:0), SM 33:1 (d18:1/15:0)]; (e) lysoPCs [lysoPC (16:0), lysoPC (18:2), lysoPC (18:0), lysoPC (18:1), lysoPC (22:0)]; (f) oxidized lipid targets ("molecule A", 7-K, OxoODE-CE, HODE-CE). Cholesterol was homogenously distributed over the entire plaque areas of both small and large lesions. CE 18:2, SMs, PCs, and oxidized lipid targets showed strong localizations in plaque of large lesion (Fig. 2A) while these signals were weak in small lesion (Fig. 2B). The localizations of lysoPCs were mostly distributed over the plaque area of small lesion (Fig. 2B). Though lysoPCs also localized across the plaque area of large lesion, it was interesting to note that strong localizations were particularly observed near the shoulder region of large atherosclerotic lesion (Fig. 2A).

To evaluate the relative abundance and distribution of detectable lipids in the sampled aortic tissues, we further analyzed the mass spectra data through multiple region of interest (ROI) analyses of detectable lipids (Fig. 3A and 4A). The relative abundance of lipids by their *p*-values were compared between randomly selected ROIs in plaque and vessel regions of the sectioned aortic tissues. The arterial media of the unaffected section of the sampled aorta was used as a control for comparison. For the large lesion (Fig. 3A), the relative abundance of targeted oxidized lipids, lysoPCs, SMs, and PCs in plaque and unaffected arterial media were significantly different. These lipids were largely distributed over the plaque area as opposed to the unaffected arterial media [Fig. 3A(i) and (ii)]. As for lysoPCs, their strong localizations at the shoulder region of atherosclerotic plaque [Fig. 3A(i) and (iii)] were distinctive and significantly different from other ROIs. Similar trends of lipid localizations were also observed in small lesion (Fig. 4A). The relative abundance of cholesterol, "molecule A", lysoPCs, SM

34:1 were significantly different from those in unaffected arterial media [Fig. 4A(i) and (ii)]. They were mostly localized in plaque and its shoulder region as opposed to the unaffected arterial media. In contrast to the localizations of lysoPC in large lesion, the distributions of lysoPCs in small lesion were strongly localized in the plaque region [Fig. 4A (ii) and (iii)].

Identification of bioactive lipids and visualization of its distributions by MS/MS imaging

Sectioned tissue was subjected to Oil Red O staining to identify the localization of neutral lipids in atherosclerotic plaque (Fig. 5A). The distributions of oxidized lipids such as oxysterols ("molecule A") or oxCEs in sectioned atherosclerotic plaque were then visualized by MS/MS imaging using iMScope (Fig. 5B) and authentic lipid standards were used to create reference MS/MS profiles (Fig. 5C). Based upon the derived MS/MS profiles, specific *m/z* of fragment ions derived from respective precursor ions of targeted oxidized lipids was used to identify and visualize each target on samples. Specific *m/z* of fragment ions used for identification of targeted lipids were as follow: 7-K and oxLig-1 at *m/z* 175 (precursor ion: *m/z* 383) [Fig. 5B (i)]; "molecule A" could be constituted of oxysterols such as 7-OH, 25-OH, or 27-OH at *m/z* 159 (precursor ion: *m/z* 367) [Fig. 5B(ii)]; and oxCEs, at *m/z* 317 and *m/z* 319 (precursor ion: *m/z* 685 and *m/z* 687) [Fig. 5B(iii) and (iv))]. By overlaying the acquired MS/MS images with their respective optical microscope image (Fig. 5B), it was discovered that the intensities of oxCEs were relatively abundant in large atherosclerotic lesion. Though CEs were extensively converted to oxidized CEs in large atherosclerotic lesion, the relatively scarce signals acquired from both 7-K and oxLig-1 may signify the ongoing process of cholesterol oxidation.

Discussions

The study of oxidized lipid metabolism is implicated as one of the pivotal elements underpinning the etiological study of lifestyle-related disease such as atherosclerosis. To date, in-depth pathophysiological assessment of lipoproteins remains rudimentary as traditional

classification approach endure limitations such as difficult handling of lipid specimens and dynamic state of lipoprotein metabolism. In order to tackle these limitations, our present study employed the use of novel iMScope system with MS/MS imaging technology to identify the presence of specific oxidized lipids in specimens of atherosclerosis study models.

MALDI-Imaging Mass Spectrometry (MALDI-IMS) was previously used by Hutchins et al. (2011) to detect CE and oxCE in human vascular lesion. The detected oxCEs were largely localized within the lesion [35]. In this study, we first used the MALDI-TOF-MS to screen several lipid targets in *Ldlr*$^{-/-}$ mice-derived nLDL and Cu^{2+}-oxLDL. We observed that CE 18:2 was only detected in nLDL but not in Cu^{2+}-oxLDL. Contrarily, oxCEs such as 9-HODE-CE and oxoODE-CE were mostly observed in Cu^{2+}-oxLDL only. These observations suggested that extensive oxidation-dependent decrement of CEs is associated with the increment of oxCEs. In addition, Cu^{2+}-modified lipid is known to have undergone extensive oxidation, hence it is worth to note that dissimilar MS profiles of presumably oxidized lipids from that of Cu^{2+}-oxLDL may signify incomplete or progressive lipid oxidation.

We subsequently used the 2-dimensional iMScope technology to visualize the distribution profiles of different lipid targets in sectioned WHHL rabbit's aortic tissues of two different sizes (small and large). CE 18:2, PCs, SMs, and the targeted oxidized lipids ("molecule A", 7-K, OxoODE-CE, HODE-CE) were strongly localized in plaque region of the sampled large atherosclerotic lesion. It was postulated that the relative abundances of these lipids were proportional to the sizes of the plaques. Aside from cholesterol and lysoPCs, low relative abundances of PCs, SMs, and oxidized lipids were observed in small atherosclerotic lesion. As the development of atherosclerotic plaque progresses gradually, these observations suggested that the processes of lipid oxidations were still in progress.

Interestingly, we observed unique distribution profiles of lysoPCs in the both small and large atherosclerotic lesions. On the large atherosclerotic lesion, the distributions of lysoPCs

were largely concentrated at the shoulder region of the plaque as opposed to the uniform distribution profiles in the small atherosclerotic plaque. It is postulated that the emergences of lysoPCs in atherosclerotic plaque may represent the onset of neo-atherosclerosis. Endothelial dysfunction is a clinical manifestation of early atherogenesis. Several reports have highlighted that the involvement of PLA_2 may contribute to inflammation and endothelial dysfunction in early atherogenesis through production of lysoPC [36, 37]. Localized PLA_2 in human atherosclerotic plaques have been shown to facilitate the production of oxidized fatty acid and lysoPC through hydrolysis of sn-2 fatty acids of oxidized phospholipids [38]. LysoPC acts as a pro-inflammatory mediator of oxidative stress and endothelial dysfunction [39]. It impedes endothelium-dependent vasodilation through downregulation of endothelial nitric oxide synthase (eNOS) mRNA expression [39] and halts the migration of endothelial cells and restoration of arterial injury [40].

We inferred that the acquisition of strong signals of lysoPCs at the shoulder region of large atherosclerotic lesion was attributed to the active enzymatic hydrolysis of PCs to lysoPCs in the region. Lipoprotein-associated phospholipase A_2 (PLA_2) is consistently generated by macrophage under oxidative stress [38]. As the phosphatide composition of LDL bio-membrane mainly consist of PC, PLA_2 hydrolyzes PC to hydroperoxide (PC-OOH), then to lysoPC and free fatty acid hydroperoxide (FFA-OOH) [41]; by hydrolyzing the sn-2 fatty acids of phospholipids and complements the formation of lysoPC and eventually to CE in later stages [42, 43].

Notably, we managed to detect and identify faint signals of 7-K, in its ionized form, from atherosclerosis plaque by MS/MS imaging. Though 7-K was the second most abundant oxysterols found in human atherosclerotic plaque after 27-OH [5], we were unable to identify the full length or other ionized form of both 7-K and oxLig-1. We speculated that the production of oxLig-1 remained scarce. As the development of atherosclerotic plaque

progresses gradually, such observation suggested that lipid oxidations were still in progress. In human, the development of atherosclerosis began at early age and it progresses over decades before it eventually reaches the vascular occlusion/rupture stage [44]. Since the detection of both 7-K and oxLig-1 by iMScope play a key part in the accomplishment of our present study, our observations suggest that an extended timepoint study using similar animal model (more than 6 months) is deemed necessary to comprehensively assess the distributions of 7-K and oxLig-1 in plaques.

On the contrary, there were also alternative inferences which may support our present findings. In human, 7-K accumulates specifically in fatty streak lesion [7]. The relatively low concentration of 7-K in atherosclerotic lesions of WHHL rabbit as reported in this study than that of human atherosclerotic plaques could be a probable inference to support the acquisition of low signal of 7-K by iMScope. In addition, it was also inferred that macrophages can initiate homeostatic regulatory mechanism to compensate cholesterol influx by promoting ATP binding cassette transporters A1 and G1 (ABCA1 and ABCG1) mediated cholesterol efflux pathways [45]. However, such compensatory mechanism is limited to non-hypercholesterolemia condition only [46]. Nonetheless, such postulation could be less important in rabbit as 27-OH, formed from cholesterol by sterol 27-hydroxylase (CYP27A1), is the most abundant oxysterol in atherosclerotic plaques [47-49]. To put all things into perspective, there is a possibility that large amount of 7-K and oxLig-1 may not be detected in atherosclerotic plaque of rabbit even if the study was performed over a longer period.

It is also worth to note that present study primarily focused on preliminary establishment and application of iMScope with MS/MS imaging technology to visualize the distributions of targeted lipids in atherosclerotic plaques. A few limitations remain to be address before such combinational technology can be put into feasible use. First of all, our data showed that the mass spectra from sectioned plaque tissue and reference standards differ from each other. Due

to the complexity of biological tissue, various co-existing biomolecules in the tissue section tend to influence the crystallization efficiency of biomolecules with the chemical matrix [50]. Such situation can negatively affect the ionization and desorption efficiency of targeted biomolecules which subsequently influence the detectable signals and profiles of mass spectra [51]; a phenomenon known as ion suppression [52]. In addition, repeated laser irradiation at similar spots during iMScope analysis often lead to loss of ion signals or ion yields. Additional instrumental optimizations in areas of laser irradiation parameters and effects of different matrices on yields of MS ion signals remain warranted to further improve the efficiency of instrumental signal acquisitions. Secondly, lipid oxidation is an ongoing process which may influence the spatial organization and integrity of lipids in biological tissues. However, in order to preserve the integrity of the biological tissue and prevent the generation of artifacts from oxidation of lipids as a result of improper sample handling, we preserved the collected aortic tissue immediately in O.C.T. compound and stored at −80°C. Thirdly, current iMScope with MS/MS imaging application focused on only one WHHL rabbit's aortic tissue that was randomly selected for analysis as a proof of concept. The technology still needs to be tested with more diverse tissue specimens, comprises of mildly and severely developed atherosclerotic plaques from pathological study model (e.g. WHHL rabbits) and non-pathological normal control models [e.g. Japanese White (JW-NIBS) strain rabbit - genetic background of WHHL rabbit] to further complement its sensitivity and specificity. Such future study will provide valuable insights especially on lipidomics and pathophysiological development of atherosclerosis.

The application of iMScope with MS/MS imaging technology offers an interesting proposition to study the pathophysiology of atherosclerotic plaque formation from the context of oxidized lipids. Based on our present findings, we were able to detect and visualize the distributions of selected oxidized lipid targets on sectioned atherosclerotic lesions. These

findings further support the applicability of iMScope as a direct approach for detection of lipid peroxides from fresh/frozen sections of tissue samples. It abolished the need for pre-analysis sample extraction, thus preserving the integrity of the specimen while keeping its susceptibility to oxidation at minimal level. At present, it is anticipated that such attempt can shed lights on identities of crucial oxidized lipids that are responsible for development and progression of atherosclerotic lesions.

Conclusions

iMScope with MS/MS imaging was successfully applied as a direct approach to analyze and visualize the distribution of targeted oxidized lipids in atherosclerotic lesions derived from atherosclerotic study models. The combination of imaging and MS/MS technology offers a valuable proposition that enables one to visualize the distributions of different lipid targets in plaques at different developmental stages.

Conflict of interest

The authors declared they do not have anything to disclose regarding conflict of interest with respect to this manuscript.

Financial support

This research was supported in part by a grant from the Ministry of Education, Culture, Sports, Science and Technology of Japan; KAKEN (Japan Society for the Promotion of Science [JSPS]), Grant Number: 26253036.

Author contributions

Shen, L. and Yamamoto, T. conducted research, performed data collection and interpretation, and manuscript preparation. Tan, X.W. assisted in data analysis and presentation, and preparation of manuscript. Ogata, K., Ando, E., and Ozeki, E. provided technical supports for application of iMScope and assisted in reviewing related data. Matsuura, E. reviewed the overall data presentation, construct of the manuscript and supported the research financially via grant-in-aid from the Ministry of Education, Culture, Sports, Science and Technology of Japan KAKEN.

Acknowledgements

The authors thank Dr. Kazuko Kobayashi, Ms. Nuriza Ulul Azmi, Dr. Arum Wahyuningsih for the critical discussion of this study, Dr. Takanori Sasaki for assisting in technicality pertaining to acquisition of rabbit aortic arches, and Ms. Yumi Unno (Analytical Applications Department, Shimadzu Corporation) for the technical supports.

References

[1] A.D. Mooradian, Dyslipidemia in type 2 diabetes mellitus, Nat. Clin. Pract. Endocrinol. Metab. 5 (2009) 150-159.

[2] W. Palinski, M.E. Rosenfeld, S. Ylä-Herttuala, G.C. Gurthner, S.S. Socher, S.W. Butler, S. Parthasarathy, T.E. Carew, D. Steinberg, J.L. Witztum, Low density lipoprotein undergoes oxidative modification *in vivo*, Proc. Natl. Acad. Sci. U.S.A. 86 (1989) 1372-1376.

[3] M. Aviram, Modified forms of low density lipoprotein and atherosclerosis, Atherosclerosis 98 (1993) 1-9.

[4] L. Nagy, P. Tontonoz, J.G.A. Alvarez, H. Chen, R.M. Evans, Oxidized LDL regulates macrophage gene expression through ligand activation of PPARγ, Cell 93 (1998) 229-240.

[5] H.S. Liao, T. Kodama, Y.J. Geng, Expression of class A scavenger receptor inhibits apoptosis of macrophages triggered by oxidized low density lipoprotein and oxysterol, Arterioscl. Throm. Vas. 20 (2000) 1968-1975.

[6] G.M. Chisolm, G. Ma, K.C. Irwin, L.L. Martin, K.G. Gunderson, L.F. Linberg, D.W. Morel, P.E. DiCorleto, 7 beta-hydroperoxycholest-5-en-3 beta-ol, a component of human atherosclerotic lesions, is the primary cytotoxin of oxidized human low density lipoprotein, P. Natl. Acad. Sci. 91 (1994) 11452-11456.

[7] A.J. Brown, W. Jessup, Oxysterols and atherosclerosis, Atherosclerosis 142 (1999) 1-28.

[8] H. Esterbauer, J. Gebicki, H. Puhl, G. Jürgens, The role of lipid peroxidation and antioxidants in oxidative modification of LDL, Free Radic. Bio. Med. 13 (1992) 341-390.

[9] A. Berthier, S. Lemaire-Ewing, C. Prunet, S. Monier, A. Athias, G. Bessède, J-P.P. de Barros, A. Laubriet, P. Gambert, G. Lizard, D. Néel, Involvement of a calcium-dependent dephosphorylation of BAD associated with the localization of Trpc-1 within lipid rafts in 7-ketocholesterol-induced THP-1 cell apoptosis, Cell Death Differ. 11 (2004) 897-905.

[10] M-C. Royer, S. Lemaire-Ewing, C. Desrumaux, S. Monier, J-P.P. de Barros, A. Athias, D. Néel, L. Lagrost, 7-ketocholesterol incorporation into sphingolipid/cholesterol-enriched (lipid raft) domains is impaired by vitamin E: a specific role for α-tocopherol with consequences on cell death, J. Biol. Chem. 284 (2009)15826-15834.

[11] O. Quehenberger, A.M. Armando, A.H. Brown, S.B. Milne, D.S. Myers, A.H. Merrill, S. Bandyopadhyay, K.N. Jones, S. Kelly, R.L. Shaner, C.M. Sullards, E. Wang, R.C. Murphy, R.M. Barkley, T.J. Leiker, C.R.H. Raetz, Z. Guan, G. M. Laird, D.A. Six, D.W. Russell, J.G. McDonald, S. Subramaniam, E. Fahy, E.A. Dennis, Lipidomics reveals a remarkable diversity of lipids in human plasma, J. Lipid Res. 51 (2010) 3299-3305.

[12] P.M. Hutchins, R.C. Murphy, Cholesteryl ester acyl oxidation and remodeling in murine macrophages: formation of oxidized phosphatidylcholine, J. Lipid Res. 53 (2012) 1588-1597.

[13] J. Belkner, H. Stender, H. Kühn, The rabbit 15-lipoxygenase preferentially oxygenates LDL cholesterol esters, and this reaction does not require vitamin E, J. Biol. Chem. 273 (1998) 23225-23232.

[14] G. Hoppe, A. Ravandi, D. Herrera, A. Kuksis, H.F. Hoff, Oxidation products of cholesteryl linoleate are resistant to hydrolysis in macrophages, form complexes with proteins, and are present in human atherosclerotic lesions, J. Lipid Res. 38 (1997) 1347-1360.

[15] C. Suarna, R.T. Dean, J. May, R. Stocker, Human atherosclerotic plaque contains both oxidized lipids and relatively large amounts of alpha-tocopherol and ascorbate, Arterioscl. Throm. Vas. 15 (1995) 1616-1624.
[16] C. Suarna, R.T. Dean, P.T. Southwell-Keeley, D.E. Moore, R. Stocker, Separation and characterization of cholesteryl oxo- and hydroxy-linoleate isolated from human atherosclerotic plaque, Free Radic. Res. 27 (1997) 397-408.
[17] J.M. Upston, X. Niu, A.J. Brown, R. Mashima, H. Wang, R. Senthilmohan, A.J. Kettle, R.T. Dean, R. Stocker, Disease stage-dependent accumulation of lipid and protein oxidation products in human atherosclerosis, Am. J. Pathol. 160 (2002) 701-710.
[18] Y. Yamamoto, M.H. Brodsky, J.C. Baker, B.N. Ames, Detection and characterization of lipid hydroperoxides at picomole levels by high-performance liquid chromatography, Anal. Biochem. 160 (1987) 7-13.
[19] Y. Kawai, A. Saito, N. Shibata, M. Kobayashi, S. Yamada, T. Osawa, K. Uchida, Covalent binding of oxidized cholesteryl esters to protein: implications for oxidative modification of low density lipoprotein and atherosclerosis, J. Biol. Chem. 278 (2003) 21040-21049.
[20] Q. Liu, K. Kobayashi, J. Furukawa, J. Inagaki, N. Sakairi, A. Iwado, T. Yasuda, T. Koike, D.R. Voelker, E. Matsuura, ω-Carboxyl variants of 7-ketocholesteryl esters are ligands for β2-glycoprotein I and mediate antibody-dependent uptake of oxidized LDL by macrophages, J. Lipid Res. 43 (2002) 1486-1495.
[21] W. Li, D. Wang, Y. Chi, R. Wang, F. Zhang, G. Ma, Z. Chen, J. Li, Z. Liu, E. Matsuura, Q. Liu, 7-ketocholesteryl-9-carboxynonanoate enhances the expression of ATP-binding cassette transporter A1 via CD36, Atherosclerosis 226 (2013) 102-109.
[22] Y. Chi, L. Wang, Y. Liu, Y. Ma, R. Wang, X. Han, H. Qiao, J. Lin, E. Matsuura, S. Liu, Q. Liu, 7-ketocholesteryl-9-carboxynonanoate enhances ATP binding cassette transporter A1 expression mediated by PPARγ in THP-1 macrophages, Atherosclerosis 234 (2014) 461-468.
[23] Y. Hasunuma, E. Matsuura, Z. Makita, T. Katahira, S. Nishi, T. Koike, Involvement of β2-glycoprotein I and anticardiolipin antibodies in oxidatively modified low-density lipoprotein uptake by macrophages, Clini. Exp. Immunol. 107 (1997) 569-573.
[24] J. George, Y. Shoenfeld, D. Harats, The involvement of β2-glycoprotein I (β2GPI) in human and murine atherosclerosis, J. Autoimmun. 13 (1999) 57-60.
[25] K. Kobayashi, M. Kishi, T. Atsumi, M.L. Bertolaccini, H. Makino, N. Sakairi, I. Yamamoto, T. Yasuda, M.A. Khamashtam, G.R.V. Hughes, T. Koike, D.R. Voelker, E. Matsuura, Circulating oxidized LDL forms complexes with β2-glycoprotein I: implication as an atherogenic autoantigen, J. Lipid Res. 44 (2003) 716-726.
[26] D. Lopez, I. Garcia-Valladares, C.A. Palafox-Sanchez, I.G. De La Torre, K. Kobayashi, E. Matsuura, L.R. Lopez, Oxidized low-density lipoprotein/β2-glycoprotein I complexes and autoantibodies to oxLig-1/β2-glycoprotein I in patients with systemic lupus erythematosus and antiphospholipid syndrome, Am. J. Clin. Pathol. 121 (2004) 426-436.
[27] E. Matsuura, K. Kobayashi, M. Tabuchi, L.R. Lopez, Oxidative modification of low-density lipoprotein and immune regulation of atherosclerosis, Prog. Lipid Res. 45 (2006) 466-486.
[28] E. Matsuura, L. Shen, Y. Matsunami, N. Quan, M. Makarova, F.J. Geske, M. Boisen, S. Yasuda, K. Kobayashi, L.R. Lopez, Pathophysiology of β2-glycoprotein I in antiphospholipid syndrome, Lupus 19 (2010) 379-384.
[29] K. Kobayashi, K. Tada, H. Itabe, T. Ueni, P-H. Liu, A. Tsutsumi, M. Kuwana, T. Yasuda, Y. Shoenfeld, P.D. de Groot, E. Matsuura, Distinguished effects of antiphospholipid antibodies and anti-oxidized LDL antibodies on oxidized LDL uptake by macrophages, Lupus 16 (2007) 929-938.

[30] T. Kajiwara, T. Yasuda, E. Matsuura, Intracellular trafficking of β2-glycoprotein I complexes with lipid vesicles in macrophages: Implications on the development of antiphospholipid syndrome, J. Autoimmun. 29 (2007) 164-173.

[31] Y. Yamaguchi, N. Seta, J. Kaburaki, K. Kobayashi, E. Matsuura, M. Kuwana, Excessive exposure to anionic surfaces maintains autoantibody response to β2-glycoprotein I in patients with antiphospholipid syndrome, Blood 110 (2007) 4312-4318.

[32] K. Kobayashi, E. Matsuura, Q. Liu, J. Furukawa, K. Kaihara, J. Inagaki, T. Atsumi, N. Sakairi, T. Yasuda, D.R. Voelker, T. Koike, A specific ligand for β2-glycoprotein I mediates autoantibody-dependent uptake of oxidized low density lipoprotein by macrophages, J. Lipid Res. 42 (2001) 697-709.

[33] L. Shen, Y. Matsunami, N. Quan, K. Kobayashi, E. Matsuura, Keiji Oguma, In vivo oxidation, platelet activation and simultaneous occurrence of natural immunity in atherosclerosis-prone mice, Isr. Med. Assoc. J. 13 (2011) 278-283.

[34] A.J. Brown, E.L. Mander, I.C Gelissen, L. Kritharides, R.T. Dean, W. Jessup, Cholesterol and oxysterol metabolism and subcellular distribution in macrophage foam cells: accumulation of oxidized esters in lysosomes, J. Lipid. Res. 41 (2000) 226-236.

[35] P.M. Hutchins, E.E. Moore, R.C. Murphy, Electrospray MS/MS reveals extensive and nonspecific oxidation of cholesterol esters in human peripheral vascular lesions, J. Lipid Res. 52 (2011) 2070-2083.

[36] S. Lavi, J.P. McConnell, C.S. Rihal, A. Prasad, V. Mathew, L.O. Lerman, A. Lerman, Local production of lipoprotein-associated phospholipase A2 and lysophosphatidylcholine in the coronary circulation, Circulation 115 (2007) 2715-2721.

[37] X. Li, P. Fang, Y. Li, Y. Kuo, A.J. Andrews, G. Nanayakkara, C. Johnson, H. Fu, H. Shan, F. Du, N.E. Hoffman, D. Yu, S. Eguchi, M. Madesh, W.J. Koch, J. Sun, X. Jiang, H. Wang, X. Yang, Mitochondrial reactive oxygen species mediate lysophosphatidylcholine-induced endothelial cell activation, Arterioscler. Thromb. Vasc. Biol. 36 (2016) 1090-1100.

[38] E.H. Yang, J.P. McConnell, R.J. Lennon, G.W. Barsness, G. Pumper, S.J. Hartman, C.S. Rihal, L.O. Lerman, A. Lerman, Lipoprotein-associated phospholipase A2 is an independent marker for coronary endothelial dysfunction in humans, Arterioscler. Thromb. Vasc. Biol. 26 (2006) 106-111.

[39] P. Kougias, H. Chai, P.H. Lin, A.B. Lumsden, Q. Yao, C. Chen, Lysophosphatidylcholine and secretory phospholipase A2 in vascular disease: mediators of endothelial dysfunction and atherosclerosis, Med. Sci. Monit. 12 (2006) RA5-16.

[40] P. Chaudhuri, S.M. Colles, D.S. Damron, L.M. Graham, Lysophosphatidylcholine inhibits endothelial cell migration by increasing intracellular calcium and activating calpain, Arterioscler. Thromb. Vasc. Biol. 23 (2003) 218-223.

[41] M. Kotosai, S. Shimada, M. Kanda, N. Matsuda, K. Sekido, Y. Shimizu, A. Tokumura, T. Nakamura, K. Murota, Y. Kawai, J. Terao, Plasma hdl reduces nonesterified fatty acid hydroperoxides originating from oxidized LDL: a mechanism for its antioxidant ability, Lipids 48 (2013) 569-578.

[42] E. Gjone, Familial lecithin: cholesterol acyltransferase (LCAT) deficiency. An updated review Spring 1988, Ophthalmic. Paediatr. Genet. 9 (1988) 167-169.

[43] M. Okita, D.C. Gaudette, G.B. Mills, B.J. Holub, Elevated levels and altered fatty acid composition of plasma lysophosphatidlycholine (lysoPC) in ovarian cancer patients, Int. J. Cancer 71 (1997) 31-34.

[44] S.M. Schwartz, K.E. Bornfeldt, How does diabetes accelerate atherosclerotic plaque rupture and arterial occlusion?, Front. Biosci. 8 (2003) s1371-s1383.

[45] X. Wang, H.L. Collins, M. Ranalletta, I.V. Fuki, J.T. Billheimer, G.H. Rothblat, A.R. Tall, D.J. Rader, Macrophage ABCA1 and ABCG1, but not SR-BI, promote macrophage reverse cholesterol transport *in vivo*, J. Clin. Invest. 117 (2007) 2216-2224.

[46] N. Shibata, C.K. Glass, Regulation of macrophage function in inflammation and atherosclerosis, J. Lipid Res. 50 (2009) S277-S281.

[47] J.M. Mathieu, J. Schloendorn, B.E. Rittmann, P.J.J. Alvarez, Medical bioremediation of age-related diseases, Microb. Cell Fact. 8 (2009) 21.

[48] I. Björkhem, O. Andersson, U. Diczfalusy, B. Sevastik, R.J. Xiu, C. Duan, E. Lund, Atherosclerosis and sterol 27-hydroxylase: evidence for a role of this enzyme in elimination of cholesterol from human macrophages, P. Natl. Acad. Sci. 91 (1994) 8592-8596.

[49] M. Crisby, J. Nilsson, V. Kostulas, I. Björkhem, U. Diczfalusy, Localization of sterol 27-hydroxylase immuno-reactivity in human atherosclerotic plaques, Biochim. Biophys. Acta 1344 (1997) 278-285.

[50] K. Chughtai, R.M.A. Heeren, Mass spectrometric imaging for biomedical tissue analysis, Chem. Rev. 110 (2010) 3237-3277.

[51] P. Chaurand, J.L. Norris, D.S. Cornett, J.A. Mobley, R.M. Caprioli, New developments in profiling and imaging of proteins from tissue sections by MALDI mass spectrometry, J. Proteome Res. 5 (2006) 2889-2900.

[52] M. Stoeckli, D. Staab, A. Schweitzer, Compound and metabolite distribution measured by MALDI mass spectrometric imaging in whole-body tissue sections, Int. J. Mass Spectrom. 260 (2007) 195-202.

[53] A. Vejux, D. Abed-Vieillard, K. Hajji, A. Zarrouk, J.J. Mackrill, S. Ghosh, T. Nury, A. Yammine, M. Zaibi, W. Mihoubi, H. Bouchab, B. Nasser, Y. Grosjean, G. Lizard, 7-ketocholesterol and 7β-hydroxycholesterol: *in vitro* and animal models used to characterize their activities and to identify molecules preventing their toxicity, Biochem. Pharmacol. 173 (2019) 113648.

Figure Legends

Fig. 1: Uptake of oxLDL by murine macrophage-like J774A.1 cells.

(A) *In vitro* intracellular lipid accumulation was studied by using the J774A.1 cells. The cells were pre-incubated with 20 μg/ml nLDL or oxLDL for 6 hours, and were subsequently analyzed by MALDI-TOF-MS. (B) The MS profiles of macrophage loaded with either nLDL or oxLDL showed product ion peaks at specific *m/z* corresponded to different lipid targets: *m/z* 369 → cholesterol ion [M+H-OH], *m/z* 383 → 7-K $[M-OH]^-$, *m/z* 401 → 7-K $[M+H]^+$, and *m/z* 367 $[M+H-2H_2O]^-$& *m/z* 385 $[M+H-H_2O]$ → "molecule A" (potentially constituted of 7-OH, 25-OH or 27-OH).

Fig. 2: MS imaging-based visual mapping profiles of oxidized lipid distributed within regions of randomly sampled atherosclerotic lesion.

Distinctive lipid profiles were observed in two different regions of sampled atherosclerotic lesion. The presented data were representatives of two regions of sectioned atherosclerotic lesion: (A) large lesion and (B) small lesion selected for analyses. A total of 6 different regions of large lesion (Supplementary Fig. 5) and 2 different regions of small lesion (Supplementary Fig. 6) were analyzed. The targeted lipids include: cholesterol; CE 18:2; PCs (PC 32:0, PC 34:2, PC 37:4, PC 36:2); SMs [SM 34:1 (18:1/16:0), SM 33:1 (d18:1/15:0)]; lysoPCs [lysoPC (16:0), lysoPC (18:2), lysoPC (18:0), lysoPC (18:1), lysoPC (22:0)]; and oxidized lipid targets ("molecule A", 7-K, OxoODE-CE, HODE-CE).

Fig. 3: Distribution profiles of lipids in large atherosclerotic lesion were studied through comparisons of relative intensities of lipids by p-values between ROI-1 and ROI-2 (A) (n = 3). The 'n' in this context denotes the number of serial tissue sections used for

analyses. Signal intensities of targeted lipids in ROI of two different regions of sampled lesion were depicted respectively and signal normalization was performed by pixel. A total of three different sets of comparisons were made: A(i) ROI-1 shoulder of atherosclerotic plaque versus ROI-2 unaffected arterial media; A(ii) ROI-1 plaque versus ROI-2 unaffected arterial media; A(iii) ROI-1 plaque region 1 versus ROI-2 plaque region 2. The letter 'p' denotes the statistical p-value of the comparison, significant differences are highlighted in green font while insignificant differences are highlighted in red font. (B) Total ion chromatograms (TIC) of MS analysis on ROI of each region of sectioned lesion. ROI for unaffected arterial media was selected from preliminary evaluations (Supplementary Fig. 7) on multiple regions of arterial media with low MS signals of cholesterol as compared to the plaque region.

Fig. 4: Distribution profiles of lipids in small atherosclerotic lesion were studied through comparisons of relative intensities of lipids by p-values between ROI-1 and ROI-2 (A) (n = 3). The 'n' in this context denotes the number of serial tissue sections used for analyses. Signal intensities of targeted lipids in ROI of two different regions of sampled lesion were depicted respectively and signal normalization was performed by pixel. A total of three different sets of comparisons were made: A(i) ROI-1 shoulder of atherosclerotic plaque versus ROI-2 unaffected arterial media; A(ii) ROI-1 plaque versus ROI-2 unaffected arterial media; A(iii) ROI-1 plaque region 1 versus ROI-2 plaque region 2. The letter 'p' denotes the statistical p-value of the comparison, significant differences are highlighted in green font while insignificant differences are highlighted in red font. (B) Total ion chromatograms (TIC) of MS analysis on ROI of each region of sectioned lesion. ROI for unaffected arterial media was selected from preliminary evaluations (Supplementary Fig. 8) on multiple regions of arterial media with low MS signals of cholesterol as compared to the plaque region.

Fig. 5: MS/MS imaging visual mapping of oxysterol and oxCEs detected on sampled WHHL rabbit atheroma.

Sectioned atherosclerotic lesion of WHHL rabbit was assessed through (A) Oil Red O staining for distribution of neutral lipids and (B) MS/MS imaging for distribution of oxidized lipids. MS/MS imaging visual mapping of targeted oxidized lipids (in green) were overlaid onto the optical microscopy image of sampled lesion (n = 3). MS/MS imaging visual mappings of targeted oxidized lipids of all sampled lesions were depicted in Supplementary Fig. 9. MS profiles of targeted oxidized lipids detected in specific regions of large atherosclerotic lesion of WHHL rabbit and their corresponding reference standards were depicted in Supplementary Fig. 3. (C) MS/MS profiles of targeted oxidized lipids detected in specific regions of large atherosclerotic lesion of the WHHL rabbits and the corresponding MS/MS profiles of reference standards of targeted oxidized lipids. "Molecule A" was postulated consisting of oxysterols such as 7-OH, 25-OH or 27-OH. Collision energies and corresponding MS/MS fragment ions of targeted oxidized lipids were presented in Table S1.

Supplementary Fig. 1: Cholesterol oxidation pathway. Oxidation of cholesterol can occur enzymatically and non-enzymatically. Enzymatic oxidation of cholesterol mostly yields esterified lipid moieties while non-enzymatic oxidation of cholesterol produces oxysterols such as 7-hydroperoxycholesterol (7-OOH) and 7-ketocholesterol (7K). Enzymatic oxidation of 7-K further yields 7-ketocholesterol ester (7-KE) and subsequent oxidation of 7-KE yields 7-ketocholesteryl-9-carboxynonanoate (oxLig-1), a major ligand for β2GPI. The reduction of 7-K to 7-OOH is catalyzed by 11β-HSD1 enzyme [53]. *Red arrow denotes the fragmentation sites of lipids. CYP27: sterol 27-hydroxylase; CYP7A: cholesterol 7 alpha-hydroxylase; 11β-HSD1/2: 11β-*

hydroxysteroid-dehydrogenase type I/ type II; LCAT: lecithin cholesterol acyltransferase; ACAT: acyl-CoA:cholesterol acyltransferase.

Supplementary Fig. 2: Oxidation of LDL was evaluated through TBARS assay. The extent of lipid oxidation was expressed in nmol MDA equivalent per mg protein.

Supplementary Fig. 3: MS spectra of authentic lipid standards. Authentic lipid standards: (**a**) cholesterol; (**B**) 27-hydroxycholesterol (27-OH); (**C**) 25-hydroxycholesterol (25-OH); (**D**) 7-hydroxycholesterol (7-OH); (**E**) 7-ketocholesterol (7-K); (**F**) 7-ketocholesteryl-9-carboxynonanoate (oxLig-1; synthesized in-house); (**G**) cholestryl linoleate (CE 18:2); (**H**) 9-hydroxy-10E,12Z-octadecadienoic acid cholestryl ester (9-HODE-CE) were analyzed by MALDI-TOF-MS and the acquired signals were represented in a plot of mass/charge ratio (*m/z*, X-axis) against their relative abundance (Y-axis).

Supplementary Fig. 4: MS profiles of lipids from nLDL and oxLDL. MS profiles of nLDL and oxLDL derived from *Ldlr*$^{-/-}$ mice were acquired by using MALDI-TOF-MS. The *m/z* values in the range of *m/z* 350-800 were measured and the zoomed-in MS profiles in the range of (**A**) *m/z* 365-405, (**B**) *m/z* 668-695, and (**C**) *m/z* 696-766 were depicted accordingly.

Supplementary Fig. 5: MS imaging-based visual mapping profiles of oxidized lipid distributed within regions of randomly sampled atherosclerotic lesion. A total 6 different regions of large lesion (A-F) were analyzed. The targeted lipids include: cholesterol; lysoPCs [lysoPC (16:0), lysoPC (18:0), lysoPC (18:2), lysoPC (18:1), lysoPC (22:0)]; SM 34:1 (18:1/16:0); and PCs [PC 32:0 (16:0/16:0), PC 37:4 (22:4/15:0)].

Supplementary Fig. 6: MS imaging-based visual mapping profiles of oxidized lipid distributed within regions of randomly sampled atherosclerotic lesion. A total 2

different regions of small lesion (A & B) were analyzed. The targeted lipids include: cholesterol; lysoPCs [lysoPC (16:0), lysoPC (18:0), lysoPC (18:2), lysoPC (18:1)]; SM 34:1 (18:1/16:0); and PCs [PC 32:0 (16:0/16:0), PC 37:4 (22:4/15:0)].

Supplementary Fig. 7: Preliminary evaluations of ROI for unaffected arterial media near region of large lesion. Multiple ROI (6 different regions) of unaffected arterial media were selected to evaluate the presence of cholesterol. ROI of unaffected arterial media was selected based on none/low MS signals of cholesterol (*m/z* 369.35) (as compared to the plaque region). MS signals of cholesterol (*m/z* 369.35) were annotated with red triangle.

Supplementary Fig. 8: Preliminary evaluations of ROI for unaffected arterial media near region of small lesion. Multiple ROI (6 different regions) of unaffected arterial media were selected to evaluate the presence of cholesterol. ROI of unaffected arterial media was selected based on none/low MS signals of cholesterol (*m/z* 369.35) (as compared to the plaque region). MS signals of cholesterol (*m/z* 369.35) were annotated with red triangle.

Supplementary Fig. 9: MS/MS imaging for distribution of oxidized lipids. MS/MS imaging visual mapping of targeted oxidized lipids were overlaid onto the optical microscopy image of sampled lesions (n = 3). MS profiles of targeted oxidized lipids detected in specific regions of large atherosclerotic lesion of WHHL rabbit and their corresponding reference standards were depicted in Supplementary Fig. 3. The insets depict the MS/MS profiles of targeted oxidized lipids detected in specific regions of large atherosclerotic lesion of the WHHL rabbits and the corresponding MS/MS profiles of reference standards of targeted oxidized lipids. “Molecule A” was postulated consisting of oxysterols such as 7-OH, 25-OH or 27-OH. Collision energies and corresponding

MS/MS fragment ions of targeted oxidized lipids were presented in Table S1.

Highlights

- We assembled a panel of oxidized lipids relating to progression of atherosclerosis
- iMScope can visualize distribution of lipid peroxides within atherosclerotic plaque
- MALDI-TOF-MS is able to characterize bioactive lipids from sectioned tissue samples
- iMScope and MALDI-TOF-MS offer novel approaches for lipidomics of atherosclerosis

Author contributions

Shen, L. and Yamamoto, T. conducted research, performed data collection and interpretation, and manuscript preparation. Tan, X.W. assisted in data analysis and presentation, and preparation of manuscript. Ogata, K., Ando, E., and Ozeki, E. provided technical supports for application of iMScope and assisted in reviewing related data. Matsuura, E. reviewed the overall data presentation, construct of the manuscript and supported the research financially via grant-in-aid from the Ministry of Education, Culture, Sports, Science and Technology of Japan KAKEN.

Graphical Abstract

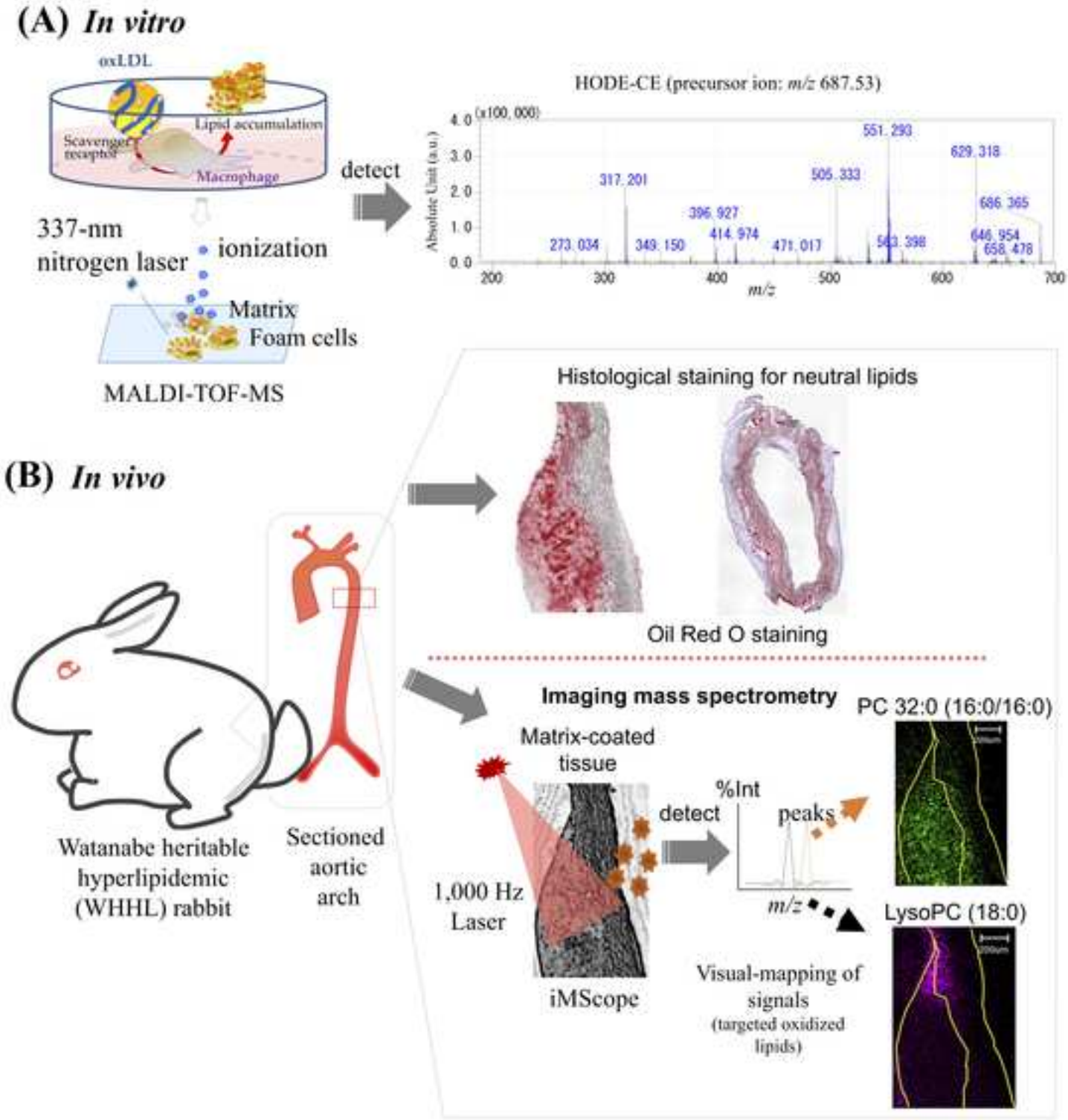

Figure 1

Click here to access/download;Figure(s);Fig. 1.jpg

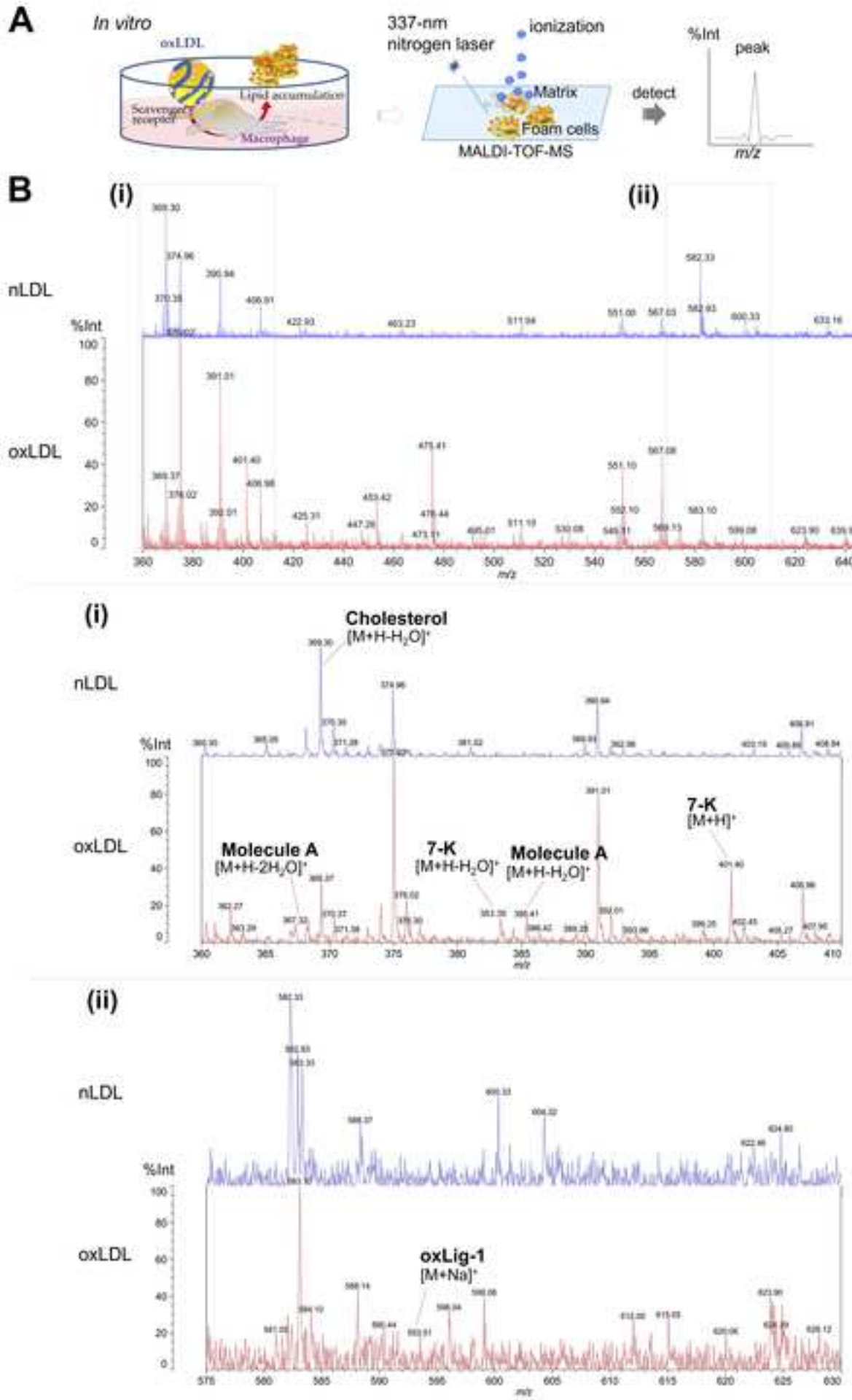

Figure 2

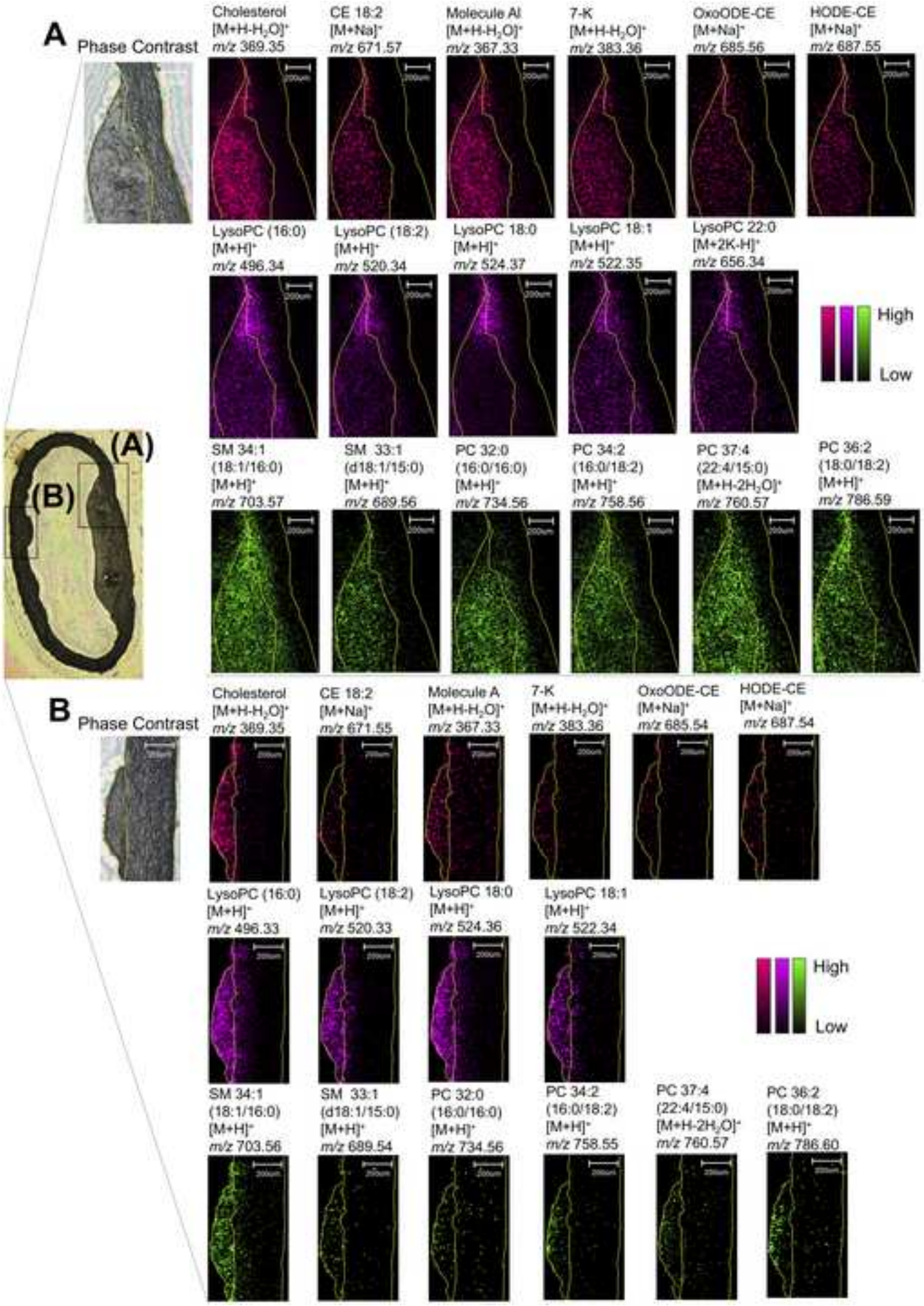

Figure 3

Click here to access/download;Figure(s);Fig. 3.jpg

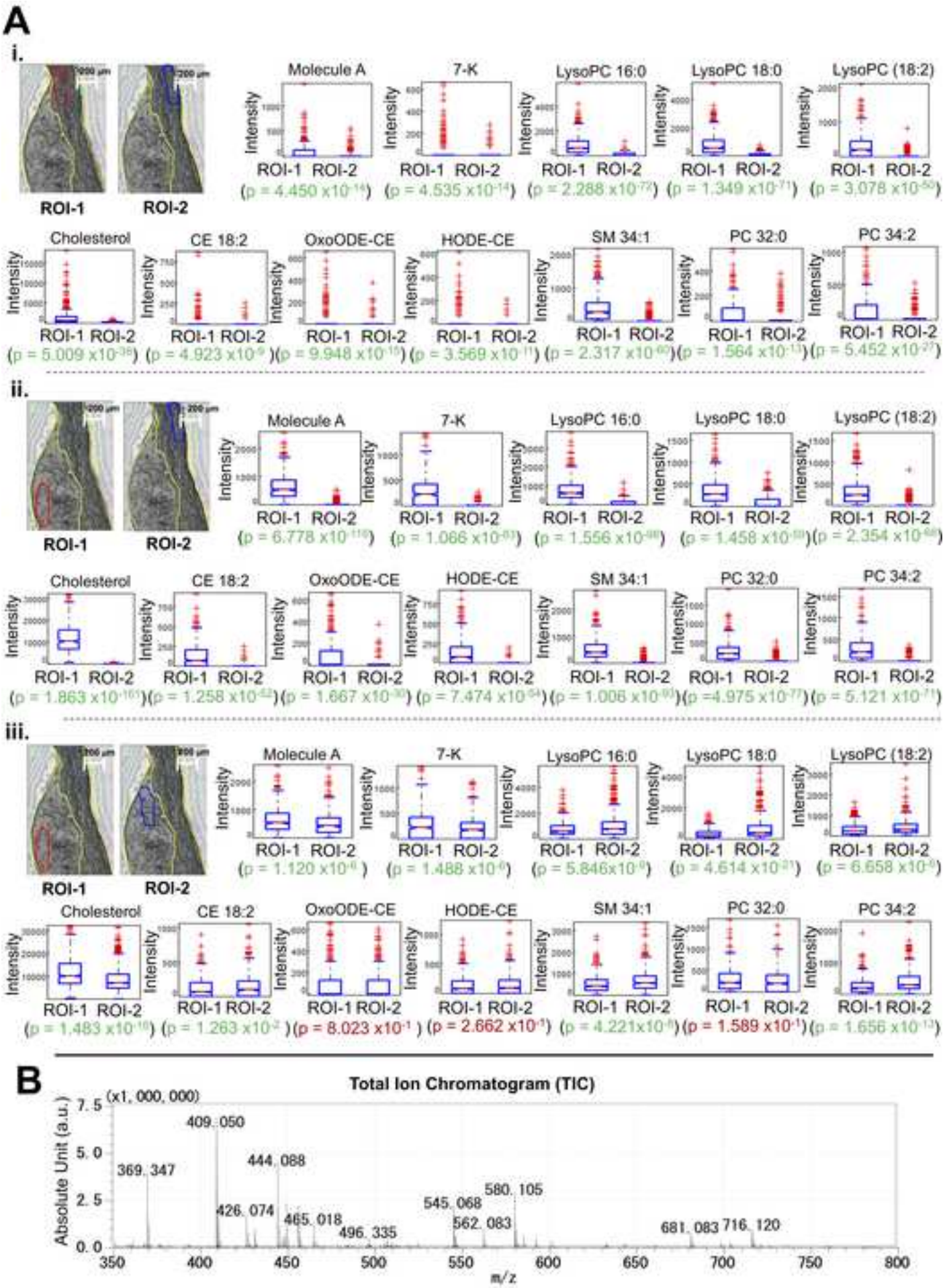

Figure 4

Click here to access/download;Figure(s);Fig. 4.jpg

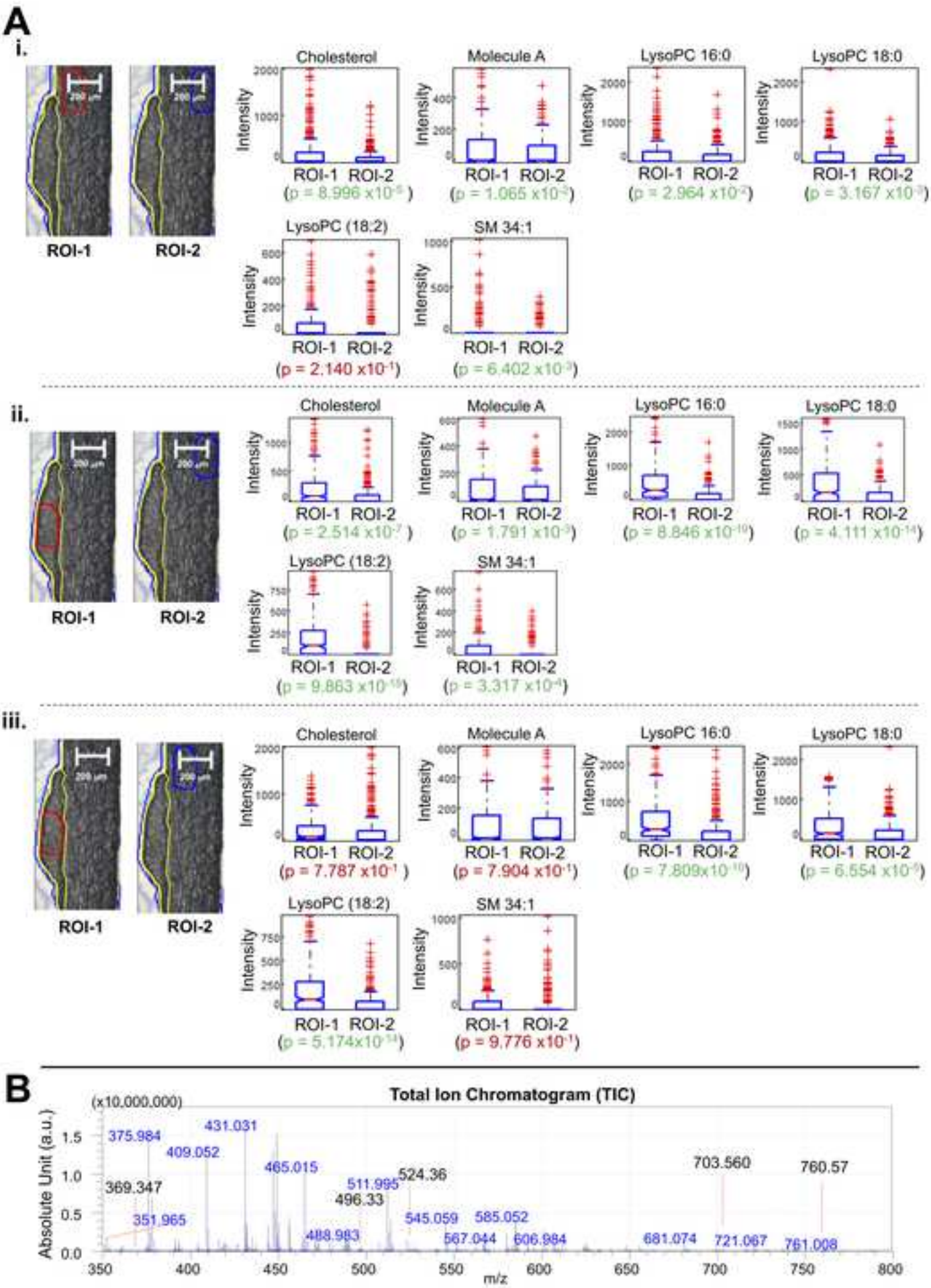

Figure 5

Click here to access/download;Figure(s);Fig. 5.jpg

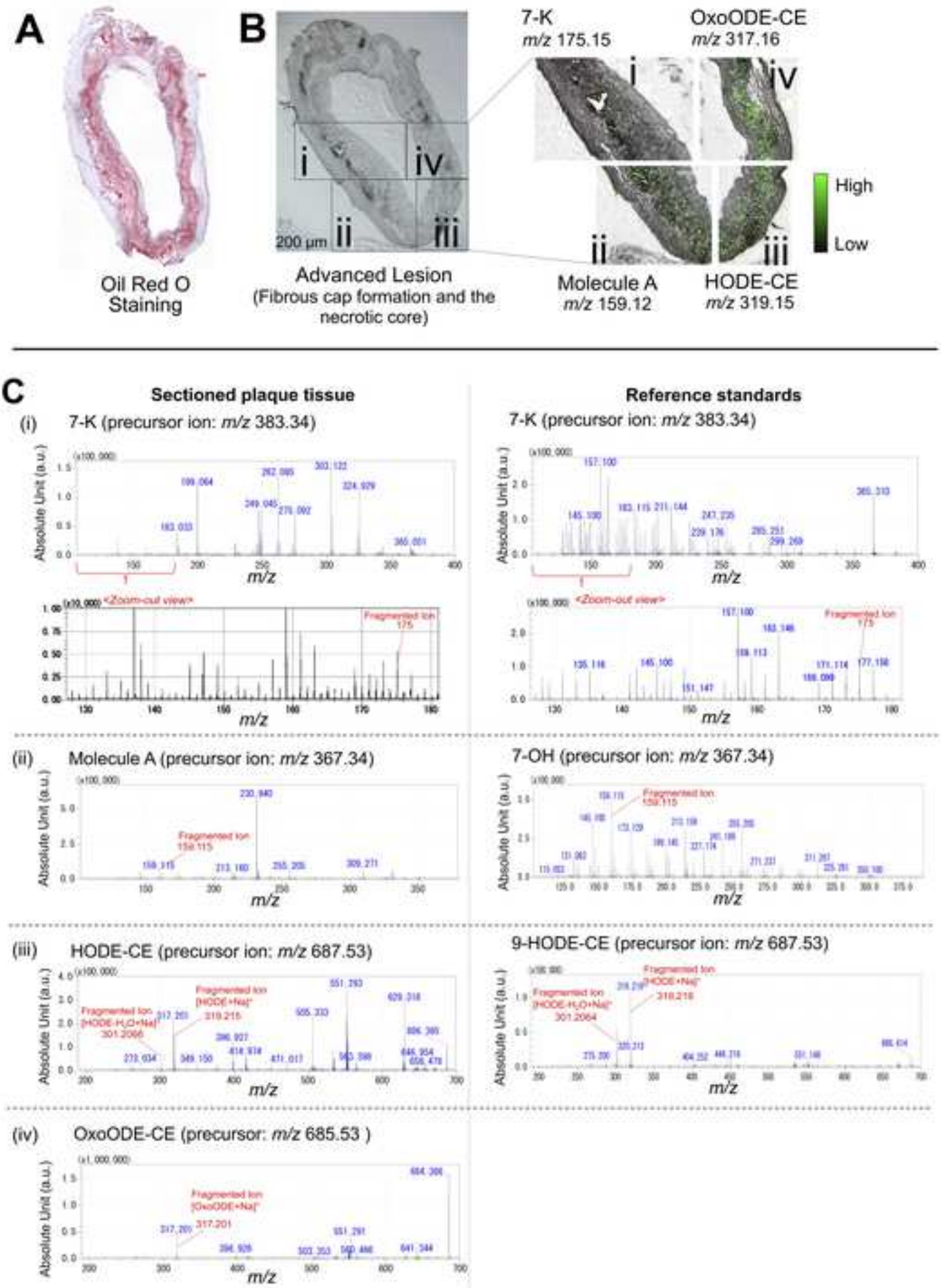

Supplementary Figure 1

Supplementary Figure 2

Supplementary Figure 3

Supplementary Figure 4

Supplementary Figure 5-1

Supplementary Figure 5-2

Supplementary Figure 6

Supplementary Figure 7

Supplementary Figure 8

Supplementary Figure 9